Asian Journal of Chemistry; Vol. 37, No. 1 (2025), 93-99

ASIAN JOURNAL OF CHEMISTRY

https://doi.org/10.14233/ajchem.2025.32843

Sustainable Porous Activated Carbon from the Bark of Wood Apple Tree as Electrode Material for Supercapacitor Application

M. SUGIRTHA[1], K. RAMESH[1,*], M. KIRUTHIGA[2], M. SARAVANAN[1], C. PRATHEEP[2] and K. SURIDHA[1]

[1]Department of Chemistry, Poompuhar College (Autonomous) (Affiliated to Bharathidasan University), Melaiyur-609107, India
[2]Department of Chemistry, Government College of Women, Kumbakonam-612001, India
[3]Department of Chemistry, King Nandhivarman College of Arts and Science, Thellar-604406, India

*Corresponding author: E-mail: rameshchemistry944@gmail.com

Received: 6 October 2024; *Accepted*: 2 December 2024; *Published online*: 31 December 2024; AJC-21855

The remarkable microstructural characteristics of porous carbons make them attractive as electrode materials for supercapacitors. The production of porous carbon from biowaste materials has gained considerable attention because of their affordability and natural abundance. This work approaches the preparation of porous carbon using the bark of wood apple tree precursor. The X-ray diffraction analysis, Fourier transform infrared spectroscopy and scanning electron microscopy techniques were performed to evaluate the physico-chemical parameters of prepared activated carbon material. In three-electrode electrochemical tests, the activated carbon WABAC3 provides the specific capacitance of 345 F g^{-1} at a current density of 1 A g^{-1} in 1 M Na_2SO_4 electrolyte with remarkable rate capability. It provides the cyclic stability of 91% of initial capacitance after 5000 continuous GCD cycles at a current density of 5 A g^{-1}.

Keywords: Activated carbon, Energy storage, Supercapacitors, Electrochemistry.

INTRODUCTION

In view of energy shortage and environmental problems brought on by an over-reliance on fossil fuels, society must progressively transition to sustainable and clean energy sources [1,2]. To preserve and utilize the captured energy wisely, renewable energies must store electric power using effective energy storage devices like batteries and supercapacitors. Supercapacitors and other cutting-edge energy storage technologies are necessary to meet the increasing requirement for portable electronics and electric cars [3]. Supercapacitors are thought to be a possible supplement for batteries because of their unique benefits, which include ultrahigh power density, exceptional cycling stability and environmental friendliness [4]. Supercapacitors exhibit potential in the automobile industry, as they provide qualities like rapid charge-discharge and high energy capacities that are essential for regenerative braking systems [5]. However, the primary drawbacks of supercapacitors are their high cost and low energy density, which severely restrict their vast range of applications. Supercapacitors with high capacitance, improved rate capability and balanced energy and power density are urgently required to fulfill the growing demands for energy storage applications.

Based on their distinct energy process, supercapacitors can be divided into two categories *viz.* electric double-layer capacitors (EDLCs) and pseudo-capacitors. Activated carbon, carbon nanotubes, graphene, carbon aerogels and carbons generated from carbides are examples of conductive carbon with high specific surface area properties, which are frequently used as electrode material for EDLCs and thus store charges *via* electrostatic interactions [6]. Metal oxides, hydroxides, sulfides and conducting polymers are used as active electrode materials in pseudocapacitors, which store electrical energy through quick redox processes [7]. For energy storage uses, carbon materials have several benefits, including their environmental friendliness, structural and morphological diversity, chemical stability against strong acids and bases and affordability. Moreover, the amphoteric features of the carbon materials lead to their natural strong electrochemical behaviour at the acceptor and donor phases. Due to their high surface area and porosity, activated carbons are regarded as the optimal choice for attaining superior capacitive and cycling performance in supercapacitors

[8]. It is now essential to produce eco-friendly alternatives to current carbon-based technology due to growing concerns about unsustainable production techniques for high-demand commodities like activated carbon [9].

Biocarbons are the solid carbon compounds made through the process of pyrolysis using biomasses as the carbon source, which have drawn more interest lately due to their potential for use in supercapacitors and other possible applications [10]. The biocarbon electrodes' porous structure and functional groups offer active sites and areas for ion storage and redox potential, significantly enhancing capacitive ability. Pyrolysis is a process that entails heating biomass to elevated temperatures in an inert atmosphere, resulting in the volatilization or decomposition of lighter components and the formation of high-carbon residues [11]. Recently, various biocarbon materials have been used as supercapacitor electrode materials. For example, the hierarchical porous activated carbon material was prepared from the cumin plant using microwave pretreatment synthetic route [12]. The resultant activated biocarbon provides a specific surface area of 1472 m^2/g and thus provides the highest specific capacitance value of 155 F g^{-1} at a current density of 0.5 mA cm^{-1} [12]. Similarly, the other activated carbons were also prepared in various biomass such as *Borassus flabellifer* flower [13], sakura flower [14], *Sapindus trifoliatus* nut shells [15], butnea monosperma [16], baobab fruit shell [17], daylily [18], aloe vera [19], willow wood [20], cabbage leaves [21] and *A. auriculiformis* tree [22] also revealed their better supercapacitor properties. Motivated by the above mentioned works, the present work demonstrates the preparation of activated carbon from the bark of wood apple tree (*Limonia acidissima*) biomass and thus used for supercapacitor application.

In this work, an activated carbon based on the biomass of tree bark of *Limonia acidissima* plant was prepared and characterized. The cyclic voltammetric (CV) and galvanostatic charge/discharge (GCD) studies were conducted to examine the supercapacitor properties.

EXPERIMENTAL

The tree bark of *Limonia acidissima* plant was collected from Mayiladuthurai district, India. Phosphoric acid (H_3PO_4) and hydrogen chloride were purchased from Sigma- Aldrich, India. N-methyl-2-pyrrolidone (NMP), potassium hydroxide and sodium sulfate were procured from SRL (India), whereas polyvinyl alcohol (PVA with molecular weight-88,000 to 97,000) was purchased from Alfa Aeser. China's Baoji Along with Filtration Material S&T Co., Ltd. was the source of the nickel foam. Deionized (DI) water was used in all of the studies in this investigation.

Methods: The freshly collected bark of wood apple tree (25 g) was washed with water several times and then dried for 2 weeks. The pieces were first dried in an oven at 100 ºC for 1 h to eliminate moisture. Afterward, they were crushed and ground to achieve the desired particle size. Phosphoric acid (50% v/v) was used as the activating agent in a chemical activation process to treat the air-dried samples. The well-dried sample was carbonized in a muffle furnace at 300 ºC for 4 h and then washed with 0.5 M HCl, followed by rinsing with hot distilled water and finally with cold distilled water until the pH of the solution become neutral. The solid carbon was then filtered and dried at 150 ºC. For doping nitrogen into the activated carbon, urea and carbon (after eliminating the acid content) were taken in a 4:1 ratio in a mortar and ground well with 10 mL of deionoized water. The obtained blend was subjected to heating at 80 ºC for 1 h. Subsequently, the mixture underwent filtration and dried at 100 ºC for 1 h. The calcination process was conducted according to the activated carbon synthesis procedure [23]. The resulting powder was referred as nitrogen-doped activated carbon. A similar process was employed for sulfur doping into activated carbon, with thiourea serving as sulfur source. The resultant activated carbon, N-doped and S-doped carbon activated materials were referred to as WABAC1, WABAC2 and WABAC3, respectively.

Characterization: A powder X-ray diffraction (XRD) study was performed on the activated carbon to investigate its crystalline characteristics. The PAN Analytical X'Pert PRO model X-ray diffractometer, which was fitted with Cu*K*α radiation (α = 1.5418 Å) and covered a 10º-80º range, was used. Using KBr as an internal standard and the pellet method, the functional groups in activated carbon were evaluated using a Perkin-Elmer FTIR spectrometer in the range of 4000–400 cm^{-1}. Utilizing the Zeiss ULTRA PLUS scanning electron microscopy (SEM), the morphological examinations were carried out.

Electrode preparation for supercapacitor analysis: The as-prepared carbon sample and PTFE were ground into a fine powder in an agate mortar at a 4:1 weight ratio in N-methyl-2-pyrollidine solvent and the resulting powder was constantly ground to obain a uniform paste. Then the paste was coated onto nickel foam (1 cm × 1cm) under the pressure of 10 MPa for 1 min. The resultant electrode was dried in a vacuum oven at 80 ºC for 12 h. Moreover, a three-electrode configuration in a 1 M Na_2SO_4 electrolyte using a CHI workstation was used to examine the electrochemical characteristics of the as-derived activated carbon electrode. Here, the carbon electrode, Ag/AgCl and platinum foil were used as active, reference and counter electrodes, respectively. To investigate the characteristics of the supercapacitor, the CV and GCD tests were carried out.

RESULTS AND DISCUSSION

XRD studies: Fig. 1 shows the XRD patterns of the prepared WABAC1, WABAC2 and WABAC3 activated carbon materials, recorded 2θ values from 0 to 50º. It is clearly observed that the two peaks have appeared in the XRD patterns. The peak at 25º is due to the (002) plane of carbon whereas the peak at 43º is due to the (100) plane of the activated carbon, respectively. The resultant two peaks are characteristic peaks of activated carbon [24]. The other peaks appeared above 40º are due to the crystalline graphitic structure of carbon, whereas the remaining peaks in the entire XRD spectra indicate the breakage of primary bond in carbon [25]. The intensities of the XRD patterns increase from WABAC1 to WABAC3 activated carbon materials, suggesting that the calcination temperature may enhance the crystalline structure of the activated carbon materials.

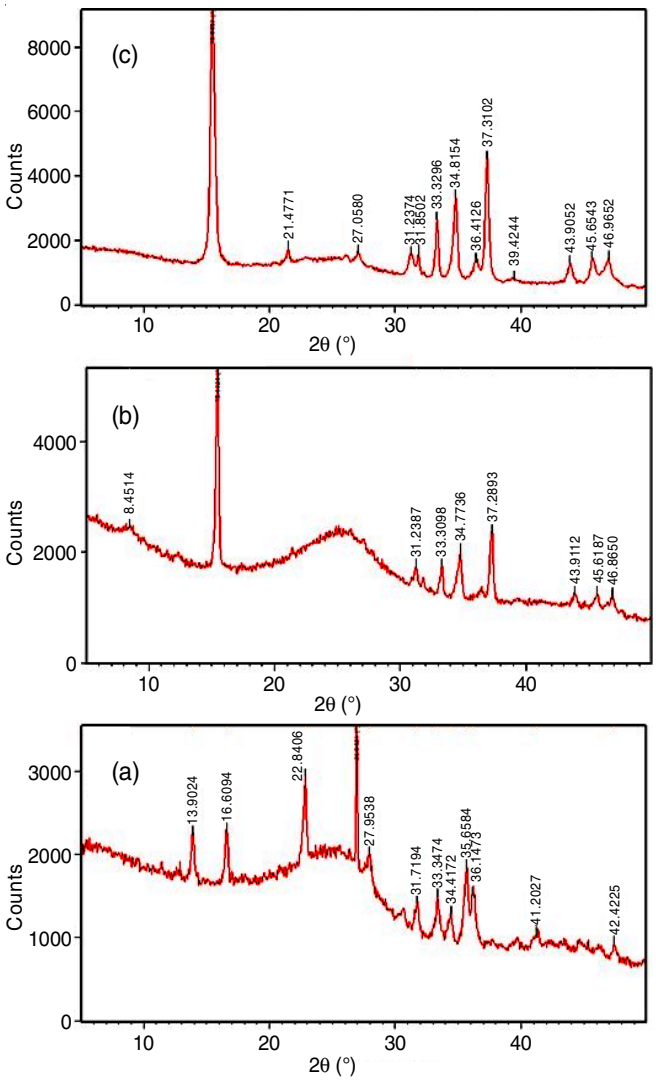

Fig. 1. XRD patterns of the (a) WABAC1, (b) WABAC2 and (c) WABAC3 materials

FTIR studies: Fig. 2a-c shows the FTIR spectra of three WABAC1, WABAC2 and WABAC3 activated carbon materials. The distinctive peaks of activated carbon, O-H bond deformation vibration and C-H stretching of aromatic compounds are confirmed in the FTIR spectra, which shows the peaks from the frequency range from 880 to 550 cm^{-1}, respectively. The functional groups detected in the activated carbon prepared from the bark of wood apple tree, closely resemble those observed in previously conducted studies for activated carbons [26]. The broad and strong peak appeared in the range between 3670 and 3200 cm^{-1} is attributed to the OH vibration. The C–H stretching of $–CH_2–$ and $–CH_3$ appeared as a wide peak in the 3200-2600 cm^{-1} frequency region. These findings verified that the broad peak is formed by the joining of the peaks from the OH and C–H stretching of the $–CH_2-$ and $–CH_3$ functional groups. The peaks in 1600-1400 cm^{-1} region are due to the C=O of the aromatic ring in the activated carbon and O–H stretching vibrations, respectively. The frequency ranges from 1200 to 1000 cm^{-1} indicating the C-O group and C-O stretching vibrations [27-30].

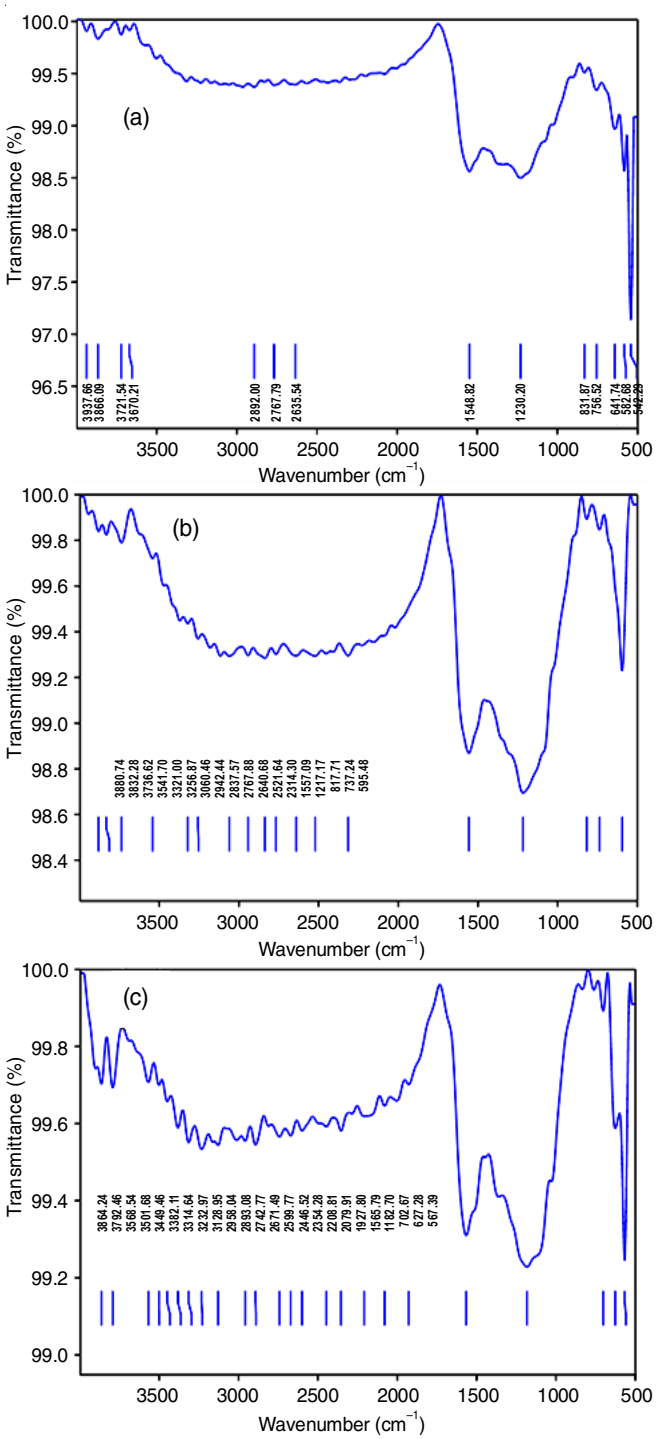

Fig. 2. FTIR analysis of the (a) WABAC1, (b) WABAC2 and (c) WABAC3 materials

Morphological studies: The surface morphological images of the WABAC1, WABAC2 and WABAC3 activated carbon materials are shown in Fig. 3a-c. The WABAC1 (Fig. 3a) material shows a wrinkled and rough morphology on the surface, which is due to surface shrinkage brought on by water evaporation, volatile substance vaporization and decomposed gaseous material decomposition during the high-temperature carbonization process. The similar pattern is also observed in the the SEM image of WABAC2 material (Fig. 3b). However,

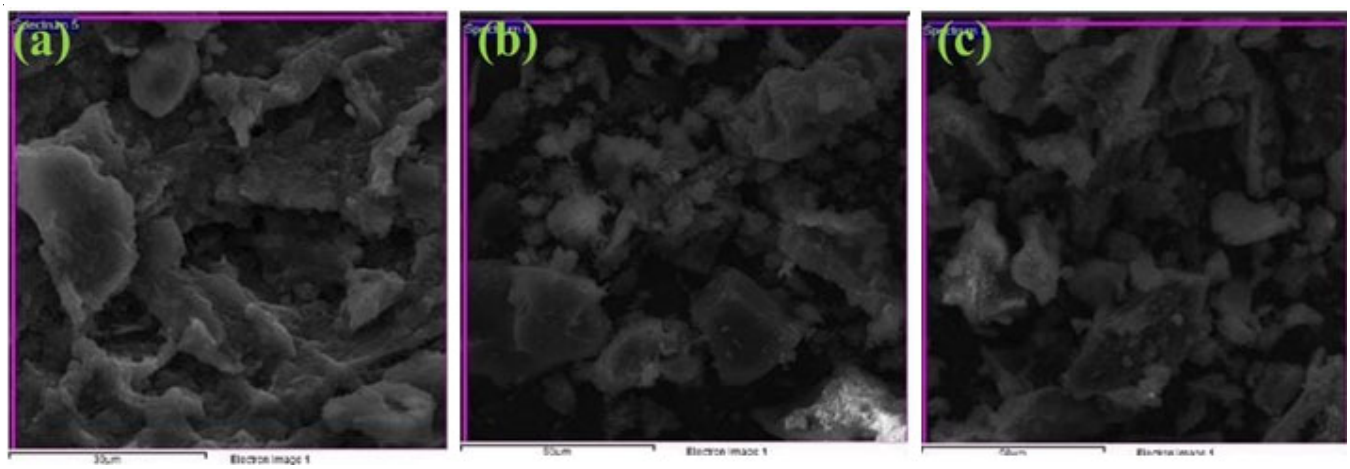

Fig. 3. SEM analysis of the (a) WABAC1, (b) WABAC2 and (c) WABAC3 materials

the size of the activated carbon materials is reduced in WABAC2 material compared to WABAC1 material, which is further reduced in WABAC3 material (Fig. 3c). This factor is attributed to the increased calcination temperature, which enhances the wrinkled and rough morphology on the surface of the activated carbon while reducing the size of the materials.

Electrochemical studies: The electrochemical properties of WABAC1, WABAC2 and WABAC3 electrodes were tested using CV and GCD studies in 1 M Na_2SO_4 electrolyte. The cyclic voltammograms of all electrodes are shown in Fig. 4a-c. The CV curves are recorded using the potential window from -1 to 0 V at various sweep rates from 5 to 100 mV s^{-1}. Before the CV analysis, all the electrodes undergo 50 CV cycles at a sweep rate of 50 mV s^{-1} to activate the electrode materials. Without any Faradaic redox peaks, all the CV curves exhibit a quasi-rectangular shape, suggesting that the electrode materials store charges using the EDLC energy storage mechanism [31]. The fact that the area under the CV curves of WABAC3 electrode (one complete cycle) is higher than the other WABAC1 and WABAC2 electrodes, suggested that the WABAC3 electrode delivers a higher specific capacitance. Maintaining a rectangular form for high scan rates implies high rate capability of cells, whereas the rectangular CV shape indicates their capacitative behaviour. Several factors could contribute to the rectangular shape observed at high scan rates. For example, tiny diffusion distance of electrolyte ions from mesopores to micropores, quick ionic transport channels inside the mesopores and the numerous sites available at the electrode surface for adsorption-desorption within micropores [32].

The GCD analyses were carried out at various current densities and are displayed in Fig. 5a-c to further validate the EDLC behaviour three electrodes *viz*. WABAC1, WABAC2 and WABAC3. The study found that compared to WABAC1 and WABAC2 electrodes, WABAC3 electrode delivers a substantially longer charge/discharge time. The GCD plots are typically shown to be triangular in pattern for EDLCs and samples with quasi-isosceles triangular GCD curves in the -1 to 1 V potential window region are indicative of a double-layer capacitance. The quasi-isosceles triangle shape observed in this case, rather than a purely triangular form, may have originated from the oxygen moiety of electrode materials, which markedly enhanced the wettability of electrode surfaces and electrochemical active sites [33]. The specific capacitance of all the GCD curves was calculated using eqn. 1:

$$\text{Specific capacitance} = \frac{I \times \Delta t}{m \times \Delta V} \quad (1)$$

where I refers to the input current density; Δt denotes discharge time; m corresponds to active material weight and ΔV denotes the current density (A g^{-1}), respectively.

The WABAC1, WABAC2 and WABAC3 electrodes show the specific capacitances of 179, 268 and 345 F g^{-1}, respectively at a current density of 1 A g^{-1}. The WABAC3 provides high specific capacitance compared to WABAC1 and WABAC2

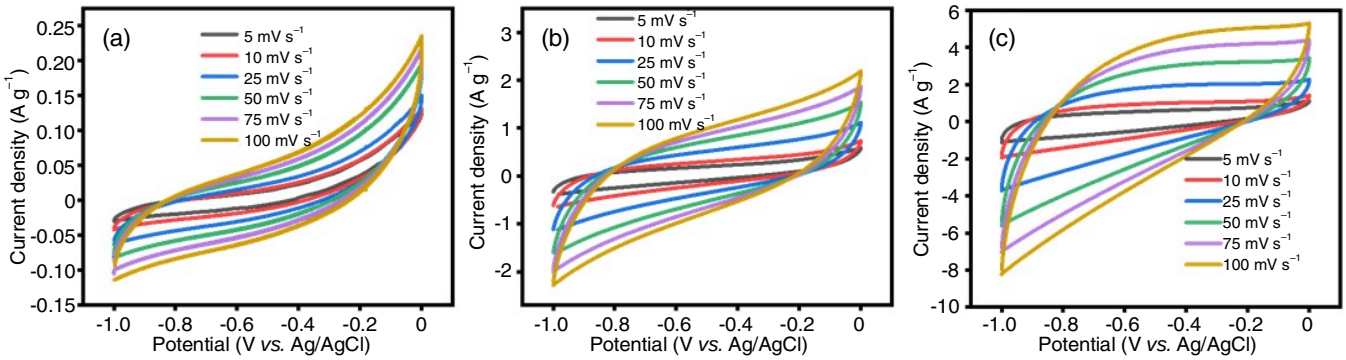

Fig. 4. CV analysis of the (a) WABAC1, (b) WABAC2 and (c) WABAC3 materials

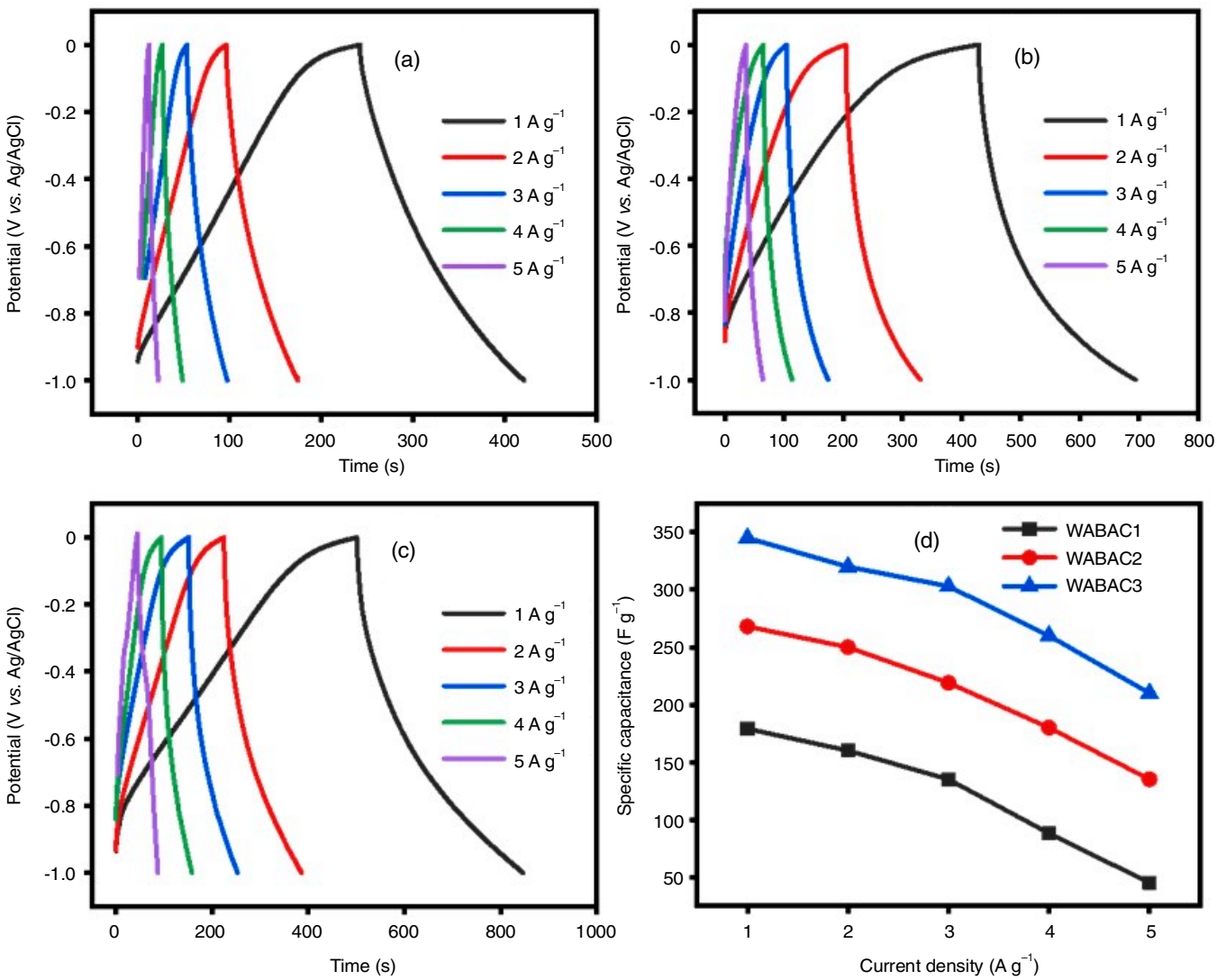

Fig. 5. GCD analysis of (a) WABAC1, (b) WABAC2 and (c) WABAC3 materials, and (d) specific capacitance *vs*. current density graph

materials. Also, the attained high specific capacitance is higher than previous literature based on biomass-derived activated carbon, as shown in Table-1.

Fig. 5d shows the specific capacitance *vs*. current density graph of WABAC1, WABAC2 and WABAC3 electrodes. It is significant to note that the specific capacitance decreases with increasing current density, which is due to the time-limiting factor. The particular capacitance behaviour is enhanced by an electrochemical process that can easily occur at a low scan rate in both the inner and exterior electrode materials. However, the short time frame makes it impossible for an electrochemical process to proceed smoothly; as a result, the outer layer of the electrode material only participates in the electrochemical process at high scan rates, which lowers the specific capacitance values.

Lastly, to assess the prepared electrode's usefulness during extended cycle usage, their cyclic stability was also examined. The cyclic stability of the WABAC1, WABAC2 and WABAC3 electrodes was evaluated using 5000 GCD cycles at a current density of 5 A g^{-1} as shown in Fig. 6. It is observed that the

TABLE-1
PERFORMANCE COMPARISON TABLE

Activated carbon from the biomass	Electrolyte	Specific capacitance (F g^{-1})	Ref.
Borassus flabellifer flower	1 M KOH	234.4 at 1 A g^{-1}	[13]
Lotus seedpod shell	3 M KOH	165 at 0.5 A g^{-1}	[33]
Sunflower seed shell	1 M KOH	311 at 125 mA g^{-1}	[34]
Waste newspaper	6 M KOH	340 at 1 A g^{-1}	[35]
Human hair	6 M KOH	305 at 1 A g^{-1}	[36]
Pomegranate rind	1 M H_2SO_4	268 at 0.1 A g^{-1}	[37]
Durian shell	1 M KOH	178 F g^{-1} at 1 mA g^{-1}	[38]
Wood apple tree bark	1 M Na_2SO_4	345 at 1 A g^{-1}	This work

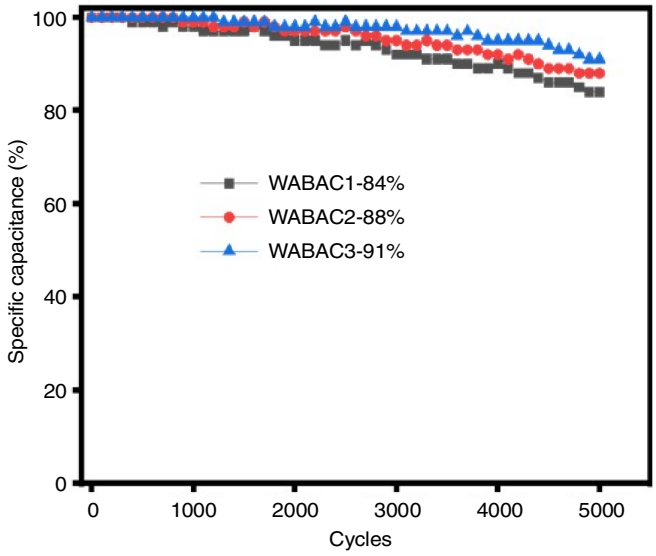

Fig. 6. Cyclic stability analysis of WABAC1, WABAC2 and WABAC3 electrodes

WABAC1, WABAC2 and WABAC3 electrodes retained 84, 88 and 91% of initial capacitance after 5000 GCD cycles, confirming that the WABAC3 electrode delivers superior cyclic stability. The reduction in capacitance retention of the electrode sample during continuous cycling is due to the blockage of micropores. Reduced ion adsorption may result from such pore obstruction and thereby decrease the values for capacitance retention. These results implied that the prepared WABAC3 material has a wide range of potential uses in low-cost energy storage device applications.

Conclusion

In summary, the activated carbon was prepared using the bark of wood apple tree at varying temperatures. The physicochemical properties were analyzed through various characterization techniques such as XRD, FTIR and SEM analysis. The specific capacitance and other parameters for different generated activated carbon materials were investigated and the impact of temperature was also observed. Sulfur doped activated carbon (WABAC3) yields a specific capacitance of 345 F g^{-1} at a current density of 1 A g^{-1} in 1 M Na_2SO_4 electrolyte with remarkable rate capability in three-electrode electrochemical experiments. At a current density of 5 A g^{-1}, it offers cyclic stability of 91% of the initial capacitance after 5000 continuous GCD cycles.

CONFLICT OF INTEREST

The authors declare that there is no conflict of interests regarding the publication of this article.

REFERENCES

1. K. Xia, Q. Gao, J. Jiang and J. Hu, *Carbon*, **46**, 1718 (2008); https://doi.org/10.1016/j.carbon.2008.07.018
2. X.Q. Lin, Q.F. Lü, Q. Li, M. Wu and R. Liu, *ACS Omega*, **3**, 13283 (2018); https://doi.org/10.1021/acsomega.8b01718
3. N. Velychkivska, A. Golunova, A. Panda, P.A. Shinde, R. Ma, K. Ariga, Y. Yamauchi, J.P. Hill, J. Labuta and L.K. Shrestha, *ACS Appl. Energy Mater.*, **7**, 2906 (2024); https://doi.org/10.1021/acsaem.4c00141
4. J. Yesuraj, V. Elumalai, M. Bhagavathiachari, A.S. Samuel, E. Elaiyappillai and P.M. Johnson, *J. Electroanal. Chem.*, **797**, 78 (2017); https://doi.org/10.1016/j.jelechem.2017.05.019
5. B. Frenzel, P. Kurzweil and H. Rönnebeck, *J. Power Sources*, **196**, 5364 (2011); https://doi.org/10.1016/j.jpowsour.2010.10.057
6. J. Yesuraj, S. Austin Suthanthiraraj and O. Padmaraj, *Mater. Sci. Semicond. Process.*, **90**, 225 (2019); https://doi.org/10.1016/j.mssp.2018.10.030
7. J. Ji, L.L. Zhang, H. Ji, Y. Li, X. Zhao, X. Bai, X. Fan, F. Zhang and R.S. Ruoff, *ACS Nano*, **7**, 6237 (2013); https://doi.org/10.1021/nn4021955
8. N. Zhao, S. Wu, C. He, C. Shi, E. Liu, X. Du and J. Li, *Mater. Lett.*, **87**, 77 (2012); https://doi.org/10.1016/j.matlet.2012.07.085
9. C. Reimer, M.R. Snowdon, S. Vivekanandhan, X. You, M. Misra, S. Gregori, D.F. Mielewski and A.K. Mohanty, *Bioresour. Technol. Rep.*, **9**, 100375 (2020); https://doi.org/10.1016/j.biteb.2019.100375
10. Y. Lu, F. Xu, L. Sun, Y. Wu, Y. Xia, X. Cai, N. Zhong, H. Zhang, B. \Li and H. Chu, *Int. J. Electrochem. Sci.*, **14**, 11199 (2019); https://doi.org/10.20964/2019.12.54
11. S. Sadaka and A.A. Boateng, Pyrolysis and Bio-Oil, Agriculture and Natural Resources, FSA1052, University of Arkansas: Fayetteville, AK, USA (2010).
12. I.I. Gurten Inal, S.M. Holmes, E. Yagmur, N. Ermumcu, A. Banford and Z. Aktas, *J. Ind. Eng. Chem.*, **61**, 124 (2018); https://doi.org/10.1016/j.jiec.2017.12.009
13. M. Sivachidambaram, J.J. Vijaya, L.J. Kennedy, R. Jothiramalingam, H.A. Al-Lohedan, M.A. Munusamy, E. Elanthamilan and J.P. Merlin, *New J. Chem.*, **41**, 3939 (2017); https://doi.org/10.1039/C6NJ03867K
14. F. Ma, S. Ding, H. Ren and Y. Liu, *RSC Adv.*, **9**, 2474 (2019); https://doi.org/10.1039/C8RA09685F
15. M. Vinayagam, R. Suresh Babu, A. Sivasamy and A.L.F. de Barros, *Carbon Lett.*, **31**, 1133 (2021); https://doi.org/10.1007/s42823-021-00235-4
16. S. Ahmed, A. Ahmed and M. Rafat, *J. Energy Storage*, **26**, 100988 (2019); https://doi.org/10.1016/j.est.2019.100988
17. A.A. Mohammed, C. Chen and Z. Zhu, *J. Colloid Interface Sci.*, **538**, 308 (2019); https://doi.org/10.1016/j.jcis.2018.11.103
18. T. Jin, J. Su, Q. Luo, W. Zhu, H. Lai, D. Huang and C. Wang, *ACS Omega*, **7**, 37564 (2022); https://doi.org/10.1021/acsomega.2c04369
19. M. Karnan, K. Subramani, N. Sudhan, N. Ilayaraja and M. Sathish, *ACS Appl. Mater. Interfaces*, **8**, 35191 (2016); https://doi.org/10.1021/acsami.6b10704
20. J. Phiri, J. Dou, T. Vuorinen, P.A.C. Gane and T.C. Maloney, *ACS Omega*, **4**, 18108 (2019); https://doi.org/10.1021/acsomega.9b01977
21. P. Wang, Q. Wang, G. Zhang, H. Jiao, X. Deng and L. Liu, *J. Solid State Electrochem.*, **20**, 319 (2016); https://doi.org/10.1007/s10008-015-3042-1
22. D. Momodu, M. Madito, F. Barzegar, A. Bello, A. Khaleed, O. Olaniyan, J. Dangbegnon and N. Manyala, *J. Solid State Electrochem.*, **21**, 859 (2017); https://doi.org/10.1007/s10008-016-3432-z
23. Z. Sitorus, Halimatuddahliana, E. Sembiring and R.F.Y. Butar-butar, *J. Phys.: Conf. Series*, **2733**, 012007 (2024); https://doi.org/10.1088/1742-6596/2733/1/012007
24. Z. Xu, T. Zhang, Z. Yuan, D. Zhang, Z. Sun, Y.X. Huang, W. Chen, D. Tian, H. Deng and Y. Zhou, *RSC Adv.*, **8**, 38081 (2018); https://doi.org/10.1039/C8RA06253F
25. S.K. Shahcheragh, M.M. Bagheri Mohagheghi and A. Shirpay, *SN Appl. Sci.*, **5**, 313 (2023); https://doi.org/10.1007/s42452-023-05559-6

26. M. Danish and T. Ahmad, *Renew. Sustain. Energy Rev.*, **87**, 1 (2018); https://doi.org/10.1016/j.rser.2018.02.003
27. S. Sharma, M. Kaur, C. Sharma, A. Choudhary and S. Paul, *ACS Omega*, **6**, 19529 (2021); https://doi.org/10.1021/acsomega.1c01830
28. J. Kaur, A.K. Sarma, M.K. Jha and P. Gera, *RSC Adv.*, **10**, 43334 (2020); https://doi.org/10.1039/D0RA08203A
29. M. Jahan and F. Feni, *Mater. Phys. Chem.*, **12**, 106 (2022); https://doi.org/10.4236/ampc.2022.125008
30. R.B.N. Lekene, D. Kouotou, N.O. Ankoro, A.P.M.S. Kouoh, J.N. Ndi and J.M. Ketcha, *J. Saudi Chem. Soc.*, **25**, 101316 (2021); https://doi.org/10.1016/j.jscs.2021.101316
31. D. Arvind and G. Hegde, *RSC Adv.*, **5**, 88339 (2015); https://doi.org/10.1039/C5RA19392C
32. Y. Liu, K. Shi and I. Zhitomirsky, *Electrochim. Acta*, **233**, 142 (2017); https://doi.org/10.1016/j.electacta.2017.03.028
33. M. Sekar, V. Sakthi and S. Rengaraj, *J. Colloid Interface Sci.*, **279**, 307 (2004); https://doi.org/10.1016/j.jcis.2004.06.042
34. X. Li, W. Xing, S. Zhuo, J. Zhou, F. Li, S.Z. Qiao and G.Q. Lu, *Bioresour. Technol.*, **102**, 1118 (2011); https://doi.org/10.1016/j.biortech.2010.08.110
35. D. Kalpana, S.H. Cho, S.B. Lee, Y.S. Lee, R. Misra and N.G. Renganathan, *J. Power Sources*, **190**, 587 (2009); https://doi.org/10.1016/j.jpowsour.2009.01.058
36. J.M. Rosas, R.Ã. Berenguer, M.Ã.J.Ã. Valero-Romero, J.Ã. Rodraguez-Mirasol and T.Ã. Cordero, *Front. Mater.*, **1**, 1 (2014); https://doi.org/10.3389/fmats.2014.00029
37. C.S. Yang, Y.S. Jang and H.K. Jeong, *Curr. Appl. Phys.*, **14**, 1616 (2014); https://doi.org/10.1016/j.cap.2014.09.021
38. K. Kanjana, P. Harding, T. Kwamman, W. Kingkam and T. Chutimasakul, *Biomass Bioenergy*, **153**, 106206 (2021); https://doi.org/10.1016/j.biombioe.2021.106206